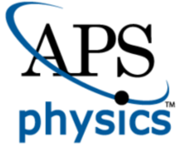

CHORUS

This is the accepted manuscript made available via CHORUS. The article has been published as:

Spin-Orbit-Torque Switching in 20-nm Perpendicular Magnetic Tunnel Junctions

Mukund Bapna, Brad Parks, Samuel D. Oberdick, Hamid Almasi, Weigang Wang, and Sara A. Majetich

Phys. Rev. Applied **10**, 024013 — Published 13 August 2018

DOI: 10.1103/PhysRevApplied.10.024013

Spin Orbit Torque Switching in 20 nm Perpendicular Magnetic Tunnel Junctions

Mukund Bapna[1], Brad Parks[1], Samuel D. Oberdick[1,2], Hamid Almasi[3], Weigang Wang[3] and Sara A. Majetich[1]*

[1]Physics Department, Carnegie Mellon University, Pittsburgh, PA
[2] Applied Physics Division, Physical Measurement Laboratory, NIST, Boulder, CO, USA
[3]Physics Department, University of Arizona, Tuscon, AZ

Keywords: Spin Orbit Torque, magnetic tunnel junction, Scanning probe microscopy

* contact author: sara@cmu.edu

Abstract

Magnetization switching utilizing the spin orbit torque of heavy metals is a promising alternative to spin transfer torque for a faster and more energy efficient write mechanism for magnetic random-access memory. We report spin orbit torque switching in a 20 nm diameter, CoFeB-MgO-based perpendicular magnetic tunnel junctions with a thermal stability factor of ~47. Conductive atomic force microscopy was used to measure the tunnel magnetoresistance before and after current pulses through the heavy metal underlayer, and magnetostatic shifts in the minor loops provided evidence of spin orbit torque switching. Comparison of estimated critical current densities and write energies suggest that spin orbit torque can be used as an effective switching mechanism for small and thermally stable perpendicular magnetic tunnel junctions.

I. Introduction

Magnetic memory, sensors, and microwave devices controlled with pure spin current or spin orbit torque (SOT) have the potential for lower power dissipation and longer lifetime than those based on spin transfer torque (STT) [1], [2]. Spin-polarized charge currents can switch a metallic nanomagnet [3], but high current densities are needed, and over time this can damage the thin tunnel barrier. Alternatively, when a charge current passes through a heavy metal conductor, a pure spin current j_s perpendicular to the charge current [4], [5] leads to SOT on the adjacent magnetic layer [6], [7] that can switch the magnetization direction [8], [9]. Switching due to spin orbit torque (SOT) has been detected through the Hall voltage or resistance [10], [11], [12] by spin torque ferromagnetic resonance (ST-FMR) [8,13–15], by the magneto-optical Kerr effect (MOKE) [16,17], and by second harmonic generation [18]. While proposed applications of the SOT involve sub-100 nm magnets, the vast majority of these experiments have been performed on larger structures because the signals are small. For example, even

when the magnetic material is several microns in diameter, the transverse spin Hall voltage is on the order of microvolts, and reducing the diameter reduces the magnitude of the signal. Many of the detection schemes require lock-in techniques, long averaging times, or angle-dependent measurements to distinguish the SOT contribution from other mechanisms [19]. Here the nanomagnet is part of a tunnel junction, and the magnetoresistance is measured by conductive atomic force microscopy (C-AFM), as shown in Figure 1. C-AFM is a point contact technique that enables electrical measurement on the patterned devices at nanoscales. This technique eliminates the need of fabrication of smaller interconnects which simplifies the overall patterning process flow for device testing at prototypical stage. We use C-AFM in measurement of spin current switching in small devices where size and surface-dependent effects may occur. For example, smaller current densities have been reported for reversal using STT in patterned films via coherent rotation in 20 nm devices than by nucleation plus domain wall motion in bigger sizes [20]. Similar differences would be expected for reversal using SOT, but only the larger structures have been measured. To date no experimental demonstration of SOT switching 20 nm or smaller perpendicular magnetic tunnel junctions (pMTJs) has been reported.

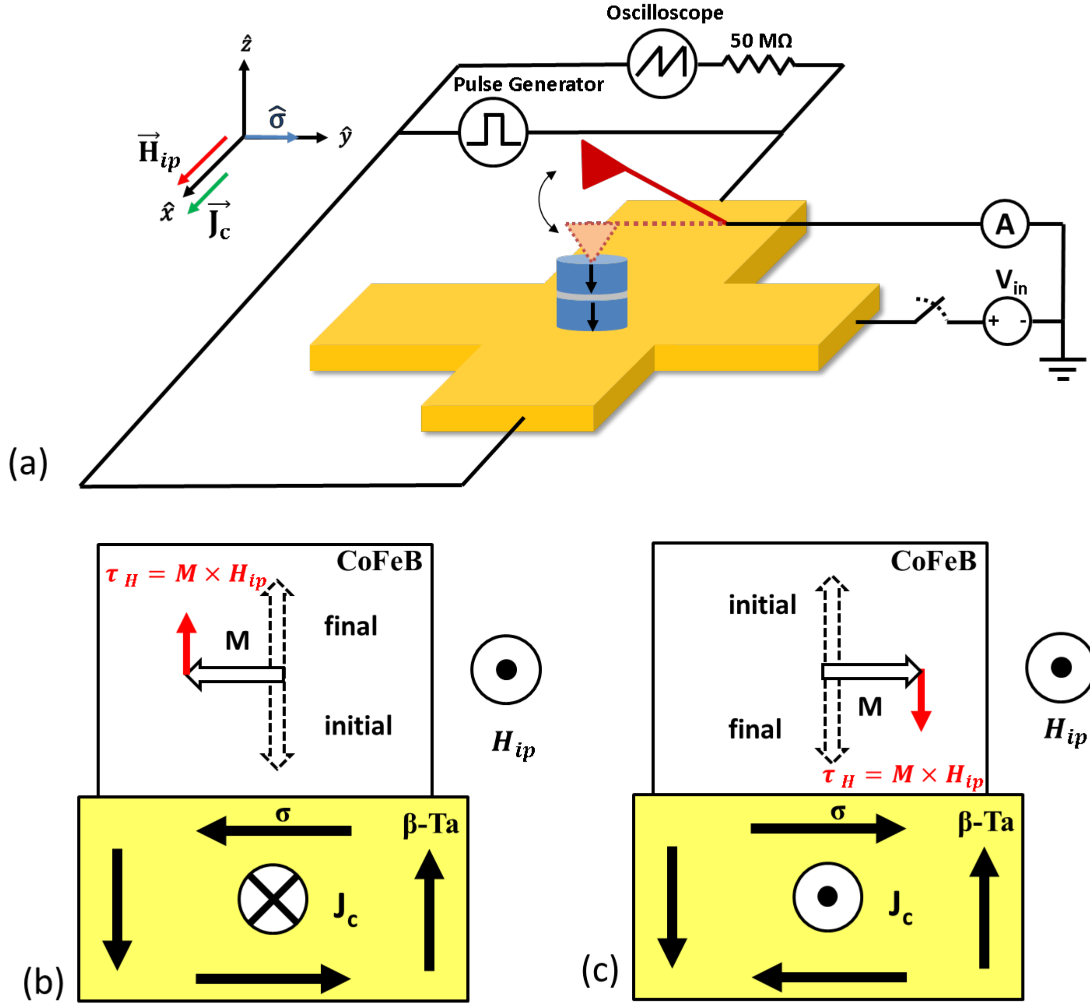

Fig 1. Schematic of the experimental setup. A charge current pulse for SOT switching and detection of the MTJ resistance state using C-AFM. A sharp conductive tip with a ~20 nm radius of curvature provides a point contact on top of the MTJ. Tunnel magnetoresistance (TMR) is measured to detect the state of the device, parallel (P) or antiparallel (AP). The tip is retracted (along $\hat{z}$) while a charge current pulse J_c (positive along $\hat{x}$) passes underneath the MTJ. The spin polarization $\hat{\sigma}$ provides torque along $\hat{y}$. The tip is brought in contact after the pulse to remeasure the TMR. The SOT pulls the magnetization in-plane and the fixed in-plane field H_{ip} determines the switching polarity as shown in (b) and (c).

II. Experimental Methods

The magnetic tunnel junction (MTJ) films in this study were deposited onto silicon wafers with 300 nm of thermal oxide in a 12-source UHV sputtering system. The deposition system is equipped with a residual gas analyzer for monitoring H_2O partial pressure and the base pressure is in the range of 10^{-9} Torr. The substrates were held at ambient temperature during deposition. The metallic layers were deposited by DC magnetron sputtering under an Ar pressure of 2 mTorr. The MgO layer was deposited by RF magnetron sputtering at 1.2 mTorr of Ar pressure. The structure of the MTJ stack is Ta(3)/Ru(5)/Ta(4)/$Co_{20}Fe_{60}B_{20}$(0.8)/MgO(1.5)/$Co_{20}Fe_{60}B_{20}$(1.5)/Ta(5)/Ru(9), where the numbers in parentheses are the film thickness in nanometers. The sample was then annealed at 300 ^{o}C for 10 min. Samples were patterned into arrays of 20-200 nm MTJs at the intersections of Hall crosses with 8.7 μm wide channels. The samples were then imaged by scanning electron microscopy (SEM) to determine the MTJ diameters. The pillars are slightly tapered, and the magnetic layers are near the bottom of the pillars. Details about the process flow can be found in Supplementary Information [21].

A conductive atomic force microscope (C-AFM) was then used to measure the resistance through the MTJ nanopillars as shown in Figure 1. The instrument was an RHK UHV350 with R9 controller operating in contact mode, in air at 300 K. Si-doped AFM probe tips (Arrow-FM nanoworld) were made conducting by sputtering 200 nm (nominal thickness) of Pt on a Ta adhesion layer. The details of these point contact measurements have been reported previously [22], [23], [24]. All C-AFM measurements were made in air and at room temperature. In all resistance measurements through the MTJ, the tip was connected to ground and the voltage refers to the voltage at the base of the MTJ, where contact was made via one of the leads to the Hall cross. The TMR as a function of magnetic field or bias was measured for individual MTJs using C-AFM. A variable out-of-plane magnetic field H_{ext} up to 1300 Oe was applied by an electromagnet directly below the sample stage.

Symmetry breaking is required for SOT reversal of a perpendicularly magnetized layer [8], [25], and so the sample was placed in the center of two permanent magnets to obtain a fixed in-plane magnetic field of 12.5 Oe along the charge current direction ($\hat{x}$) as is shown in Figure 1. The effect of the SOT is to cant the magnetization towards the spin polarization direction σ. When the magnetization points towards the spin polarization direction, which is along the hard axis or the in-plane axis of the free layer, an external field is needed to break symmetry for deterministic switching as shown in Figure 1 (b) and (c). In the SOT switching experiments, C-AFM was used to record the tunnel magnetoresistance (TMR) as a function of field before and after current pulses through the Hall cross. In between, the tip was retracted by 100 nm in the $\hat{z}$ direction and the sample was isolated from the C-AFM voltage source. This charge current was produced using a Global Specialties 4001 Ultravariable pulse generator, used in voltage-controlled and single shot mode. The voltage was fixed at 8 V and the pulse width 200 μs, with rise and fall times less than 15 ns. An external oscilloscope (Tektronix model TDS 3032) with a 50 MΩ terminator was connected in parallel to the Hall cross to monitor the voltage drop. This, together with the resistance measured by a multimeter (~200 Ω), was used to determine the charge current. After establishing the minimum charge current and pulse duration needed to observe SOT switching in the smallest devices, these parameters were kept constant for the remaining experiments. We then varied the current direction and the magnitude and direction ($\pm\hat{z}$) of the out-of-plane magnetic field. The perpendicular magnetic field was necessary both to initialize the MTJ in an AP state, and also to help in deterministic switching of the high anisotropy bottom CoFeB layer using SOT.

III. Results and Discussion

A. pMTJ Imaging

Figure 2 shows three images of the sample: an optical image of the Pt leads leading to a β-Ta Hall cross, a scanning electron microscopy (SEM) image of an array of MTJs within the Hall cross intersection, and a C-AFM current map of the nanopillars.

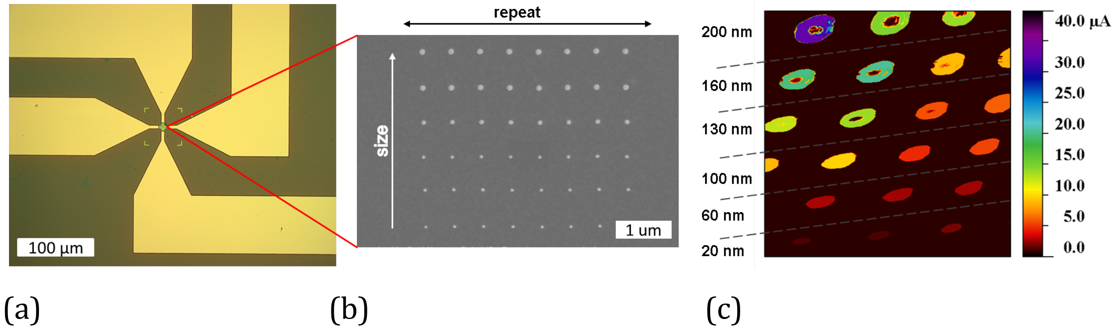

(a) (b) (c)

Fig. 2. (a) Optical image of photo-lithographically patterned Pt leads leading to a Hall cross. (b) SEM image of an MTJ array in one of the Hall crosses, with pillar diameters of 20, 60, 100, 130, 160, and 200 nm (bottom to top). The pillar height was 16 nm. (c) C-AFM current map of the same nanopillars, taken at 20 mV bias. The sizes obtained from SEM are shown at the side. The scan size is 4 µm x 4 µm.

Figure 2c shows the MTJ pillars when imaged by CAFM at low bias voltage, with H = 0. The color reflects the total amount of current passing from the Hall cross through to the C-AFM tip. The background has virtually no current because the surface of the β-Ta has oxidized. For a constant RA product, more current flows through a pillar with a larger diameter. The apparent size of the colored pillars is bigger than the mentioned lateral sizes that we found using SEM imaging due to the large tip radius of curvature of 200 nm of wear resistant tips used for CAFM imaging here. To make point contacts and for electrical measurements 20 nm MTJs CAFM tips with 20 nm tip radius of curvature were used. The RA product corresponding to the low resistance state measured at 10 mV was 6.2 $\Omega\mu m^2$. We see uniform conductivity across individual devices. The apparently non-conducting regions seen in the conductivity map for larger devices are an artifact, due to residual resist. Note that in several cases (100, 130, and 160 nm), there are two different current levels for devices of the same

diameter. This arises because even without initialization, some of the MTJs are in the P state while others are in the AP state.

B. SOT Switching of pMTJs

The applied field of the in situ electromagnet was not large enough to obtain major loops with reversal of both the top and bottom layers; therefore, an indirect method was used to determine the magnetization direction of the bottom CoFeB layer. This was achieved by measuring a minor loop for the top layer, where the loop shift (positive or negative) gives the direction of stray field (down or up) due to the bottom layer. If the top layer direction is unchanged, but SOT switches the bottom layer, the magnetostatic loop shift direction reverses.

Figure 3 illustrates how the current maps and minor loops change following SOT switching. Figure 3 (a) shows an SEM image of the 20 nm device, and Figure 3 (b) and (c) show the current maps for the MTJ before and after the current pulse through the Ta underlayer. Minor loops of the resistance as a function of the applied magnetic field are also shown for the same 20 nm pMTJ, for two different directions of the bottom layer magnetization. A loop shift of 161 Oe was observed for this device size, similar observations were predicted in our previous work on magnetostatic effects in patterned pMTJs [23]. The method of using loop shifts to determine magnetization direction have also been previously utilized in magnetic multilayer systems [26,27]. In between the measurements shown in Figure 3 (d) and (e), a perpendicular field of +100 Oe was maintained, and a charge current pulse (200 μs, 40 mA) was passed through the heavy metal layers beneath the MTJ, switching the bottom layer. We did not observe any switching without the external out-of-plane field, suggesting the torque due to the SOT alone was not sufficient to cause magnetization reversal at 40 mA. The role of external out-of-plane field here is to reduce the required current density for SOT switching [28]. Once a switch was observed, checks were made to be sure it was not due to thermal activation. No

switch was seen when initialized in the same AP state with the opposite current direction. However, switches were observed when both the bottom layer magnetization and the current direction were reversed. This is consistent with expectations for SOT switching, but not for thermally assisted switching, which would be random, or for an Oersted field from the current pulse, where switching would be independent of the current direction. These data illustrate two advantages of using a MTJ in SOT switching experiments. The tunnel magnetoresistance (TMR) is 128%, and resistance changes between 20 and 50 kΩ for the two states, unlike with Hall resistance measurements, where the typical differences range from mΩ to Ω, requiring lock-in techniques and angle-dependent measurements to differentiate SOT switching from other phenomena.

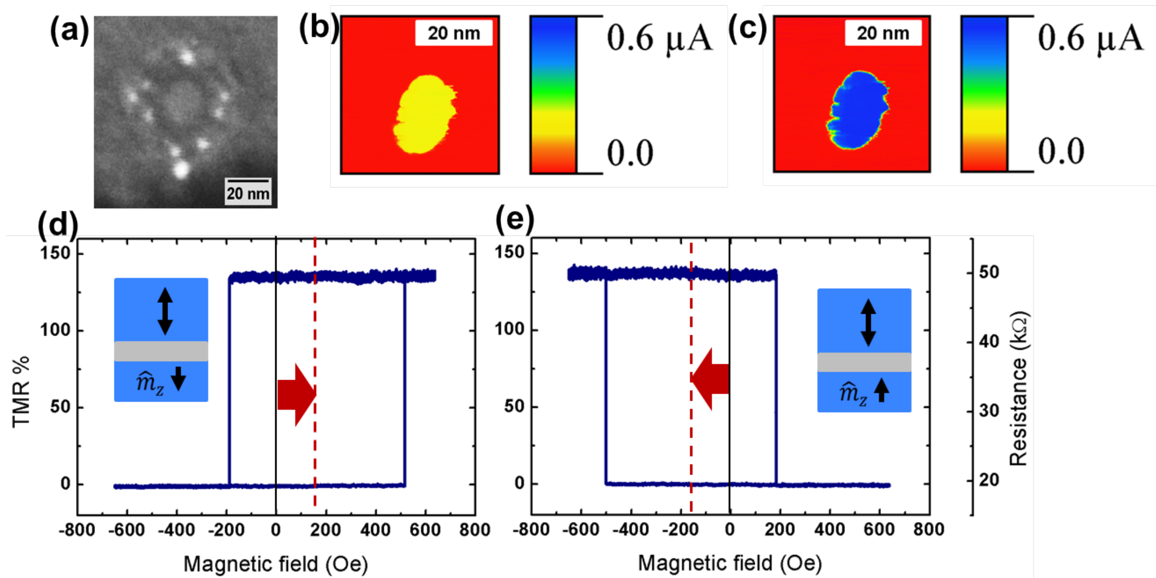

Fig. 3. (a) SEM image of a 20 nm device. Current maps measured using C-AFM of the device initially in the AP state (b), and after SOT switching to the P state (c). Minor loop resistance for the 20 nm MTJ at 10 mV bias, showing different loop shift directions before (d) and after (e) the current pulse. The top layer coercivity is 353 Oe and the loop shift is 161 Oe.

High current densities required to observe SOT switching is potentially troublesome for low power applications of the SOT. In our switching experiments, the current amplitude is large because of the Ru layer below the Ta in the Hall cross base. The electrical resistivity of Ru ~ 7.6 μΩcm [29], [30] is however much smaller than for β-Ta ~ 190 μΩcm [9], so the vast majority of the current flows through the Ru and contributes minimally to the SOT. Since Ru is a 4d metal and the strength of spin-orbit coupling scales as Z^4, Ru is expected to be far less efficient at transforming charge current to spin current than Ta. Moreover, the spin diffusion length in Ru is less than 4 nm [31], and so Ru would act as a sink for spin current generated in the bottom Ta layer. Assuming uniform electrical contact through the bonding pad, and ignoring oxidation, COMSOL simulations indicate a current density of 3.35 x 10^6 A/cm^2 in the top Ta layer, and an additional 38% reduction in current density at the center of the cross, where the MTJs are located [21]. Similar reductions have been reported elsewhere [17]. The effective charge current density generating the spin current for switching is estimated to be $J_c^{SOT} = 2.39 \times 10^6$ A/cm^2, which is comparable to values typical of STT reversal, but without having to pass large current through the MTJ.

A second factor that impacts the SOT charge current amplitude is the high anisotropy of the adjacent CoFeB layer. Because major loops could not be measured, the effective anisotropy $K_{eff,bottom}$ was estimated indirectly. $K_{eff,top}$ was found from switching field distributions of minor loops measured multiple times [21], and related to the interface anisotropy K_i, using a method that has been described previously [24]. The interface anisotropy K_i was determined from $K_i / t = K_{eff} + |K_b| + |K_s|$, where t is the thickness. Thickness dependent measurements on similar single magnetic layer films grown by the authors indicated M_s=1150 emu/cc and a reduced K_b= 8.3 erg/cc [32]. With a top layer thickness of 1.5 nm, K_i=1.4 erg/cm^2, and assuming the same K_i for the bottom layer, with thickness t = 0.8 nm leads to $K_{eff,bottom} = 8.2$ erg/cc. The PMA at the Fe/MgO interface is largely determined by the hybridization of Fe 3d orbitals and O 2p orbitals. In our MTJ stack

with large TMR, careful control of the oxidation level results in the high K_{eff} value that we observe here [33] [32]. If the bottom layer were considered as an isolated particle, its thermal stability factor Δ_{bottom} = 47±2 and the anisotropy field is $H_{eff,\ bottom} = 14.3\ \pm 1.3$ kOe.

C. Estimation of field-free critical current densities and write energies

The experiments reported here were done in a magnetic field, both to reduce the current requirements and to have deterministic switching, but by correcting for field effects it is possible to compare SOT and STT switching. The vast majority of the demonstrations of SOT switching have been performed on MTJs with in-plane magnetization or a partial in-plane component. With pMTJs, a symmetry-breaking element is required for deterministic switching [17,34]. The SOT causes the out-of-plane magnetization to be pulled in-plane. Once the magnetization is in-plane switching can then be achieved either stochastically by external perturbations such as thermal effects, or deterministically by simultaneous application of an in-plane field. Deterministic switching can also be achieved through the STT effect [17], [18]. STT-assisted SOT switching is predicted to reduce the switching time and critical current density [17,34,35].

In our experiments an out-of-plane external field $H_{z,ext}$=100 Oe, far less than the anisotropy field $H_{eff,\ bottom} = 14.3\ \pm 1.3$ kOe, was used to demonstrate deterministic switching, but we can estimate the STT current that would be needed for field-free reversal. In a three terminal device, the torque coming from STT would correspond to an additional current density $J_{add}^{STT} = \frac{2e}{\hbar} \cdot \frac{\alpha\ t_f M_s}{P} \cdot H_{z,ext} = 6.64 \times 10^4 A/cm^2$ through the device. Here e is the electron charge, $\hbar$ is Planck's constant, the damping parameter $\alpha = 0.015$ [36], the film thickness $t_f = 0.8\ nm$, M_s=1150 emu/cc and the spin polarization factor $P = 0.62$, calculated using Julliere formula TMR=2P^2/(1-P^2) with TMR=128%. In contrast, for a device with thermal stability Δ=47, the critical switching current density for pure STT switching is expected to be

$J_{c0}^{STT} = \frac{2e}{\hbar} \cdot \frac{\alpha \ t_f M_s}{\eta} \cdot H_{eff} = 6.3 \times 10^6 A/cm^2$. In our case $(J_{add}^{STT} + J_c^{SOT})/J_{c0}^{STT} \approx 0.36$, suggesting a reduction in the required current density is feasible using a STT-assisted SOT scheme.

We can also estimate the write energy per bit. From an application viewpoint, we assume an array of 20 nm devices, with 50 nm device-to-device distances on a 4 nm thick, 50 nm wide β-Ta channels. For SOT with deterministic switching, the switching time is estimated to be <10 ns [17,34]. As discussed above, switching can be achieved with $J_c^{SOT} = 2.39 \times 10^6$ A/cm^2 through β-Ta with 190 μΩcm resistivity and $J_{add}^{STT} = 6.64 \times 10^4 A/cm^2$ through a pMTJ with R = 20 kΩ. This yields energy consumption per switch in a cell $E_{sw}^{SOT+STT} = \sum I^2 Rt \approx 0.1$ fJ. Here the contribution due to the power dissipation from the STT current through the pMTJ is less than 10%. In contrast, the required energy per switch for the same cell using *only* STT current is estimated to be $E_{sw}^{STT} \approx 0.3$ pJ. Moreover, with STT switching the charge current passes through the high resistance MTJ, while with SOT switching it flows only through the heavy metal. When a charge current pulse travels through the Hall cross, all of the MTJs are exposed to the same spin current density. Hence multiple devices can be switched with the same voltage and current density, whereas such a scheme is impractical using STT due to high series resistance that the tunnel barriers would add. SOT could provide a dramatic reduction in energy consumption; however, challenges remain in fabricating such devices at scales where size-dependent effects may occur [21] and with proper interconnects to allow a three terminal read and write.

IV. Summary

In summary, this work represents the smallest known and thermally stable perpendicular magnetic device switched using SOT, more than 300 times smaller area than in the pioneering demonstration of Miron [8]. Our CAFM technique of switching detection based on TMR readout and magnetostatic loop shift is a simple

way to detect switching in small devices with a large signal-to-noise ratio. The effective SOT charge current density through the Ta underlayer was less compared to that typical for STT reversal. Moreover, with field or STT assisted scheme such devices can be switched at much lower energy per write as compared to the conventional STT scheme.

Acknowledgments

This work was supported in part by STARnet, a Semiconductor Research Corporation project sponsored by MARCO and DARPA, under contract no 2013-MA-2831, and by NSF grant ECCS-1709845 .

References

[1] A. Brataas, A. D. Kent, and H. Ohno, Current-induced torques in magnetic materials, Nat. Mater. **11**, 372 (2012).
[2] C. F. Pai, L. Liu, Y. Li, H. W. Tseng, D. C. Ralph, and R. A. Buhrman, Spin transfer torque devices utilizing the giant spin Hall effect of tungsten, Appl. Phys. Lett. **101**, 122404 (2012).
[3] J. Katine, F. Albert, R. Buhrman, E. Myers, and D. Ralph, Current-Driven Magnetization Reversal and Spin-Wave Excitations in Co /Cu /Co Pillars, Phys. Rev. Lett. **84**, 3149 (2000).
[4] E. Saitoh, M. Ueda, H. Miyajima, and G. Tatara, Conversion of spin current into charge current at room temperature, Inverse spin-Hall effect. Appl. Phys. Lett. **88**, 182509 (2006).
[5] K. Ando, S. Takahashi, K. Harii, K. Sasage, J. Ieda, S. Maekawa, and E. Saitoh, Electric manipulation of spin relaxation using the spin hall effect, Phys. Rev. Lett. **101**, 036601 (2008).
[6] M. I. D'yakonov and V. I. Perel', Possibility of orienting electron spins with current, JETP Lett. **13**, 467 (1971).
[7] J. E. Hirsch. Spin Hall Effect, Phys. Rev. Lett. **83**, 1834 (1999).
[8] I. M. Miron, K. Garello, G. Gaudin, P.-J. Zermatten, M. V Costache, S. Auffret, S. Bandiera, B. Rodmacq, A. Schuhl, and P. Gambardella, Perpendicular switching of a single ferromagnetic layer induced by in-plane current injection, Nature **476**, 189 (2011).
[9] L. Liu, C.-F. Pai, Y. Li, H. W. Tseng, D. C. Ralph, and R. A. Buhrman, Spin-Torque Switching with the Giant Spin Hall Effect of Tantalum, Science (80) **336**, 555 (2012).
[10] Y. Kajiwara, K. Harii, S. Takahashi, J. Ohe, K. Uchida, M. Mizuguchi, H. Umezawa, H. Kawai, K. Ando, K. Takanashi, S. Maekawa, and E. Saitoh, Transmission of electrical signals by spin-wave interconversion in a magnetic insulator, Nature **464**, 262 (2010).
[11] K. Garello, I. M. Miron, C. O. Avci, F. Freimuth, Y. Mokrousov, S. Blügel, S. Auffret, O. Boulle, G. Gaudin, and P. Gambardella, Symmetry and magnitude of spin–orbit torques in ferromagnetic heterostructures, Nat. Nanotechnol. **8**, 587 (2013).
[12] C. Zhang, S. Fukami, H. Sato, F. Matsukura, and H. Ohno, Spin-orbit torque induced magnetization switching in nano-scale Ta/CoFeB/MgO, Appl. Phys. Lett. **107**, 12401 (2015).
[13] L. Liu, T. Moriyama, D. C. Ralph, and R. A. Buhrman, Spin-torque ferromagnetic resonance induced by the spin Hall effect, Phys. Rev. Lett. **106**, 036601 (2011).
[14] D. Fang, H. Kurebayashi, J. Wunderlich, K. Výborný, L. P. Zârbo, R. P. Campion, A. Casiraghi, B. L. Gallagher, T. Jungwirth, and A. J. Ferguson, Spin–orbit-driven ferromagnetic resonance. Nat. Nanotechnol. **6**, 413 (2011).
[15] S. I. Kiselev, J. C. Sankey, I. N. Krivorotov, N. C. Emley, R. J. Schoelkopf, R. A. Buhrman, and D. C. Ralph, Microwave oscillations of a nanomagnet driven by a spin-polarized current, Nature **425**, 380 (2003).

[16] G. Yu, P. Upadhyaya, K. L. Wong, W. Jiang, J. G. Alzate, J. Tang, P. K. Amiri, and K. L. Wang, Magnetization switching through spin-Hall-effect-induced chiral domain wall propagation, Phys. Rev. B **89**, 104421 (2014).
[17] A. van den Brink, G. Vermijs, A. Solignac, J. Koo, J. T. Kohlhepp, H. J. M. Swagten, and B. Koopmans, Field-free magnetization reversal by spin-Hall effect and exchange bias, Nat. Commun. **7**, 10854 (2016).
[18] A. Pattabi, Z. Gu, J. Gorchon, Y. Yang, J. Finley, O. J. Lee, H. A. Raziq, S. Salahuddin, and J. Bokor, Direct optical detection of current induced spin accumulation in metals by magnetization-induced second harmonic generation, Appl. Phys. Lett. **107**, 152404 (2015).
[19] J. Wunderlich, Current-switched magnetic insulator, Nat. Mater. **16**, 284 (2017).
[20] M. Gajek, J. J. Nowak, J. Z. Sun, P. L. Trouilloud, E. J. O'Sullivan, D. W. Abraham, M. C. Gaidis, G. Hu, S. Brown, Y. Zhu, R. P. Robertazzi, W. J. Gallagher, and D. C. Worledge, Spin torque switching of 20 nm magnetic tunnel junctions with perpendicular anisotropy, Appl. Phys. Lett. **100**, 132408 (2012).
[21] See Supplemental Material at [URL] for details on Hall cross fabrication process flow, COMSOL simulations, switching field ditributions and variation of Hc and TMR with size.
[22] S. K. Piotrowski, M. F. Matty, and S. A. Majetich, Magnetic fluctuations in individual superparamagnetic particles, IEEE Trans. Magn. **50**, 2303704 (2014).
[23] M. Bapna, S. K. Piotrowski, S. D. Oberdick, M. Li, C.-L. Chien, and S. A. Majetich, Magnetostatic effects on switching in small magnetic tunnel junctions, Appl. Phys. Lett. **108**, 22406 (2016).
[24] S. K. Piotrowski, M. Bapna, S. D. Oberdick, S. A. Majetich, M. Li, C. L. Chien, R. Ahmed, and R. H. Victora, Size and voltage dependence of effective anisotropy in sub-100-nm perpendicular magnetic tunnel junctions, Phys. Rev. B-Condensed Matter **94**, 14404 (2016).
[25] D. MacNeill, G. M. Stiehl, M. H. D. Guimaraes, R. A. Buhrman, J. Park, and D. C. Ralph, Control of spin–orbit torques through crystal symmetry in WTe2/ferromagnet bilayers, Nat. Phys. **13**, 300 (2016).
[26] V. Grolier, D. Renard, B. Bartenlian, P. Beauvillain, C. Chappert, C. Dupas, J. Ferré, M. Galtier, E. Kolb, M. Mulloy, J. P. Renard, and P. Veillet, Unambiguous evidence of oscillatory magnetic coupling between Co layers in ultrahigh vacuum grown Co/Au(111)/Co trilayers, Phys. Rev. Lett. **71**, 3023 (1993).
[27] M. Matczak, L. Frackowiak, P. Kuswik, M. Urbaniak, B. Szymanski, and F. Stobiecki, Magnetization Reversal and Domain Replication in Co–Au–Co Film with Perpendicular Anisotropy, IEEE Trans. Magn. **50**, 1 (2014).
[28] L. Liu, O. J. Lee, T. J. Gudmundsen, D. C. Ralph, and R. A. Buhrman, Current-Induced Switching of Perpendicularly Magnetized Magnetic Layers Using Spin Torque from the Spin Hall Effect, Phys. Rev. Lett. **109**, 096602 (2012).
[29] S. Dutta, K. Sankaran, K. Moors, G. Pourtois, S. Van Elshocht, J. Bömmels, W. Vandervorst, Z. Tokei, and C. Adelmann, Thickness dependence of the resistivity of platinum-group metal thin films, J. Appl. Phys. **122**, 25107 (2017).

[30] J. W. Arblaster, Selected Electrical Resistivity Values for the Platinum Group of Metals Part III: Ruthenium and Osmium, Johnson Matthey Technol. Rev. **60**, 179 (2016).
[31] S. Yakata, Y. Ando, T. Miyazaki, and S. Mizukami, Temperature dependences of spin-diffusion lengths of Cu and Ru layers, Japanese J. Appl. Physics, Part 1 Regul. Pap. Short Notes Rev. Pap. **45**, 3892 (2006).
[32] H. Almasi, C. L. Sun, X. Li, T. Newhouse-Illige, C. Bi, K. C. Price, S. Nahar, C. Grezes, Q. Hu, P. Khalili Amiri, K. L. Wang, P. M. Voyles, and W. G. Wang, Perpendicular magnetic tunnel junction with W seed and capping layers, J. Appl. Phys. **121**, 153902 (2017).
[33] H. Almasi, M. Xu, Y. Xu, T. Newhouse-Illige, and W. G. Wang, Effect of Mo insertion layers on the magnetoresistance and perpendicular magnetic anisotropy in Ta/CoFeB/MgO junctions, Appl. Phys. Lett. **109**, 32401 (2016).
[34] Z. Wang, W. Zhao, E. Deng, J.-O. Klein, and C. Chappert, Perpendicular-anisotropy magnetic tunnel junction switched by spin-Hall-assisted spin-transfer torque, J. Phys. D. Appl. Phys. **48**, 65001 (2015).
[35] K.-S. Lee, S.-W. Lee, B.-C. Min, and K.-J. Lee, Threshold current for switching of a perpendicular magnetic layer induced by spin Hall effect, Appl. Phys. Lett. **102**, 112410 (2013).
[36] T. Devolder, P. H. Ducrot, J. P. Adam, I. Barisic, N. Vernier, J. Kim, B. Ockert, and D. Ravelosona, Damping of Co x Fe 80−x B 20 ultrathin films with perpendicular magnetic anisotropy, Appl. Phys. Lett. **102**, 22407 (2013).